

a sublethal dose for this strain of *L. monocytogenes*, were injected intravenously. The titer of viable bacteria in the inoculum and in organ homogenates was determined by plating 10-fold serial dilutions on trypticase soy agar plates. Eta-1<sup>-/-</sup> mice contained liver-associated *Listeria*-infected cysts that were apparent 4 to 5 days after infection. Plates were incubated at 37°C, and the numbers of CFU were counted after 24 hours.

24. Spleen cells (4 × 10<sup>6</sup>/ml) from four to five C57BL/6 × 129 Eta-1<sup>+/+</sup> or four to five C57BL/6 × 129 Eta-1<sup>-/-</sup> mice that had been intravenously inoculated 5 days earlier with 10<sup>3</sup> CFU were stimulated with heat-killed *L. monocytogenes* (2 × 10<sup>8</sup> CFU/ml) 96 hours before IFN-γ measurement by an OptEIA ELISA kit (PharMingen).

25. P. Stordeur et al., *Mol. Immunol.* **32**, 233 (1995); P. Stordeur and M. Goldman, *Int. Rev. Immunol.* **16**, 501 (1998).

26. G. F. Weber, S. Ashkar, M. J. Glimcher, H. Cantor, *Science* **271**, 509 (1996).

27. L. Liaw et al., *J. Clin. Invest.* **95**, 713 (1995); D. R. Senger et al., *Am. J. Pathol.* **149**, 293 (1996).

28. Addition of 5 mM GRGDS peptide but not GRADS peptide (29) to cultures of peritoneal macrophages (38) resulted in an 80% reduction of the IL-12 response after LPS stimulation.

29. Single-letter abbreviations for the amino acid residues are as follows: A, Ala; D, Asp; E, Glu; G, Gly; L, Leu; N, Asn; P, Pro; Q, Gln; R, Arg; S, Ser; and T, Thr.

30. R. Schmits et al., *Blood* **90**, 2217 (1997).

31. T. Kubota et al., *Biochem. Biophys. Res. Commun.* **162**, 1453 (1989); A. F. Chambers, E. I. Behrend, S. M. Wilson, D. T. Denhardt, *Anticancer Res.* **12**, 43 (1992); E. S. Sorensen and T. E. Petersen, *Biochem. Biophys. Res. Commun.* **198**, 200 (1994); H. Salih, S. Ashkar, L. C. Gerstenfeld, M. J. Glimcher, *J. Biol. Chem.* **272**, 13966 (1997).

32. M. Nemir, M. W. DeVouge, B. B. Mukherjee, *J. Biol. Chem.* **264**, 18202 (1989); B. Ek-Rylander, M. Flores, M. Wendel, D. Heinegard, G. Andersson, *J. Biol. Chem.* **269**, 14853 (1994).

33. Dephosphorylation of Eta-1 is as follows. Five milligrams of purified Eta-1 was dephosphorylated using 6 U (60 U/mg) of type-II potato acid phosphatase (Sigma) as described (39). Phosphorylation of recombinant Eta-1:glutathione S-transferase (GST)-Eta-1 (5 mg) was phosphorylated as described [S. Ashkar, J. L. Schaffer, E. Salih, L. C. Gerstenfeld, M. J. Glimcher, *Ann. N.Y. Acad. Sci.* **760**, 296 (1995); (27)]. Phosphoamino acid analysis of the recovered protein revealed a phosphoserine content of 16 mol of phosphate per 1 mol of protein and 0.8 mol of phosphothreonine per 1 mol of protein.

34. S. L. Constant and K. Bottomly, *Annu. Rev. Immunol.* **15**, 297 (1999).

35. B. M. Segal, B. K. Dwyer, E. M. Shevach, *J. Exp. Med.* **187**, 537 (1998).

36. A. Lyons, J. L. Kelly, M. L. Rodrick, J. A. Mannick, J. A. Lederer, *Ann. Surg.* **226**, 450 (1997); J. L. Kelly, A. Lyons, C. C. Soberg, J. A. Mannick, J. A. Lederer, *Surgery* **122**, 146 (1997).

37. Z. Yin et al., *Arthritis Rheum.* **40**, 1788 (1997).

38. PVP-dependent granulomas were formed as follows. C57BL/6 (+/+), C57BL/6 *nu/nu*, C57BL/6-IL-12<sup>-/-</sup> C57BL/6 × 129 Eta-1<sup>+/+</sup>, and C57BL/6 × 129 Eta-1<sup>-/-</sup> mice were injected subcutaneously above the right hind limb with 500 μl of 0.5% PVP; C57BL/6 *nu/nu* and Eta-1<sup>-/-</sup> mice were coinjected with this inoculum of PVP and 10 μg of Eta-1 and purified as described below. After 5 days, mice were killed, tissue was extracted for histologic analysis, and local lymph nodes were obtained for cytokine expression. Samples were fixed in 10% buffered formalin and embedded in paraffin; 4- to 5-μm serial sections were stained with hematoxylin and eosin, and images were captured with a Sony DXC-970MD video camera and Optima 5.2 Histomorphometric analysis software.

39. S. Ashkar et al., *Biochem. Biophys. Res. Comm.* **191**, 126 (1993).

40. Recombinant GST-Eta-1 fusion protein derived from *Escherichia coli* was digested with factor Xa and purified by affinity chromatography [S. Ashkar, M. J. Glimcher, R. A. Saavedra, *Biochem. Biophys. Res. Commun.* **194**, 274 (1993); (39)]. Briefly, native Eta-1 was isolated

from MC3T3E1 cells or Ar5v T cells after concentration in PBS using a Millipore tangential flow system, applied to a Millipore LC100 equipped with a DEAE-Memsep 1000 cartridge, and developed in a discontinuous gradient of 0 to 1 M NaCl in phosphate buffer (pH 7.4). Eta-1-containing fractions were pooled (the major Eta-1 peak eluted at 0.26 M salt), concentrated by ultrafiltration, chromatofocused on mono P columns (Pharmacia) at pH 8.2, developed with polybuffer 74 (Pharmacia), and eluted from monobeads at pH 4.6. The eluted protein was judged to be pure by several criteria, including SDS electrophoresis and amino acid sequence analysis (NH<sub>2</sub>-terminal and internal peptide analysis). Mass spectroscopic analysis revealed a peak centered around a mass of 35,400 daltons that was highly phosphorylated (11 mol of phosphate per 1 mol of protein), O-glycosylated but not N-glycosylated, and without measurable sulfate.

41. Resident peritoneal macrophages obtained by peritoneal lavage with phosphate-buffered saline (PBS) were treated with red cell lysis buffer and incubated (10<sup>5</sup> macrophages per 100 μl) for 2 hours. The adherent fraction was incubated with 5 nM Eta-1, LPS (30 ng/ml), or recombinant IL-4 (500 U/ml), or as indicated. Supernatant IL-10 or IL-12 p70 was assayed with commercial ELISA kits (R&D Systems, Minneapolis, MN), tested for viability by propidium iodide (>98%), and stained with fluorescein-conjugated antibody to Mac-1 (>98%). Blocking antibody to integrin β<sub>3</sub> was from PharMingen [J. F. Schultz and D. R. Armant, *J. Biol. Chem.* **270**, 11522 (1995)], and

antibody to CD44, KM81 (ATCC), was used to block the interaction between CD44 and Eta-1 (16).

42. Although partial tryptic, chemotryptic, or Asp-N endopeptidase digestion of Eta-1 did not reveal an active peptide, a 10-kD fragment isolated from a Lys-C digest [NH<sub>2</sub>-terminal sequence QETLPSN (29)] was active and predicted to terminate at the thrombin cleavage site. This 10-kD fragment contained ~5 mol of phosphate per 1 mol of peptide at seven potential phosphorylation sites.

43. Supported in part by NIH research grants AI12184, AI37833 (to H.C.), CA76176 (to G.F.W.), and AR34078 (to M.J.G.); grants AR44434, DC01295, ES06897 (to D.T.D.), and CA72740 (to S.R.R.) for development of Opn-null mice at Rutgers University; U.S. Department of Defense breast cancer grants DAMD17-98-1-8060 (to G.F.W.) and DAMD 17-99-1-9124 (to S.A.); U.S. Department of Public Health grant 340B9930002 and Biomorphics (to S.A.); the Fulbright Foundation (to S.Z.); and the Swedish Foundation for International Cooperation in Research and Higher Education (to M.J.). All experimentation involving animals was in accordance with Dana-Farber institutional guidelines. We thank T. W. Mak for CD44<sup>-/-</sup> mice; B. J. Rollins for *L. monocytogenes* strain 1778; S. Hikita and D. Block for technical assistance; and A. Angel, K. MacKay, and L. Lagasse for assistance in the preparation of the manuscript.

21 October 1999; accepted 15 December 1999

## Synaptic Assembly of the Brain in the Absence of Neurotransmitter Secretion

Matthijs Verhage,<sup>1,2,\*</sup> Ascanio S. Maia,<sup>1</sup> Jaap J. Plomp,<sup>3</sup> Arjen B. Brussaard,<sup>4</sup> Joost H. Heeroma,<sup>1</sup> Hendrika Vermeer,<sup>1</sup> Ruud F. Toonen,<sup>1</sup> Robert E. Hammer,<sup>5</sup> Timo K. van den Berg,<sup>6</sup> Markus Missler,<sup>2†</sup> Hans J. Geuze,<sup>7</sup> Thomas C. Südhof<sup>2\*</sup>

Brain function requires precisely orchestrated connectivity between neurons. Establishment of these connections is believed to require signals secreted from outgrowing axons, followed by synapse formation between selected neurons. Deletion of a single protein, Munc18-1, in mice leads to a complete loss of neurotransmitter secretion from synaptic vesicles throughout development. However, this does not prevent normal brain assembly, including formation of layered structures, fiber pathways, and morphologically defined synapses. After assembly is completed, neurons undergo apoptosis, leading to widespread neurodegeneration. Thus, synaptic connectivity does not depend on neurotransmitter secretion, but its maintenance does. Neurotransmitter secretion probably functions to validate already established synaptic connections.

Synapses are focal points of communication between nerve cells. Together, billions of synapses account for the unique connectivity of the brain (1). To establish the synaptic network, outgrowing axons are precisely directed to their targets using a variety of guidance cues and recognition signals on the outgrowing axon and the target cell (2). Fusion of neurotransmitter vesicles at the axon tip is believed to supply the membrane for axonal outgrowth (3). The concomitant neurotransmitter release is thought to have a trophic role and to provide essential signals for the correct targeting of axons and synapse formation:

Components of the presynaptic secretion machinery are already expressed in immature neurons before they differentiate (4). These components are targeted to the axon tip, where they are thought to be essential for axonal outgrowth in vitro (3, 5). Outgrowing neurons have an active synaptic vesicle cycle, secrete neurotransmitters before synapse formation, and up-regulate this secretion once the growth cone comes close to its target (6). After synapses have formed, the secretion capacity of nerve terminals is up-regulated, and the Ca<sup>2+</sup> affinity and tetanus toxin sensitivity increase.

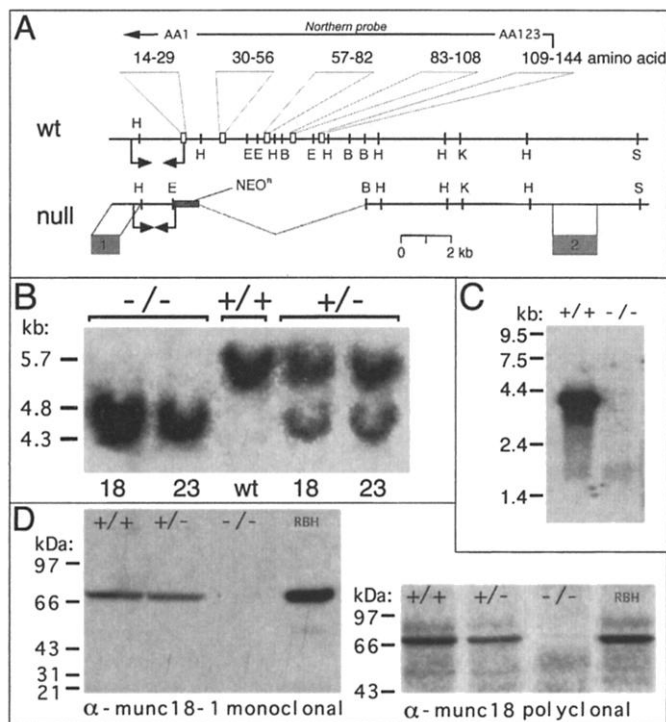
## REPORTS

Many genes have been identified that function in neurotransmitter secretion at mature synapses (7), and drastic phenotypes have been observed upon deleting such genes in mice (8). However, all currently known

gene deletions do not impair normal brain development. This can be explained by the fact that only certain aspects of the presynaptic function are abolished in these mutants. In particular, spontaneous, quantal transmit-

ter release is retained even in the most severely affected mutants (9). We have now identified the *munc18-1* gene as an essential gene for all components of neurotransmitter release throughout the brain. Munc18-1/nSec1 (10) is a neuron-specific protein of the SEC1-family of membrane-trafficking proteins. Munc18-1 is expressed throughout the brain and interacts with at least three classes of proteins, which suggests that it may regulate cell polarization as well as focal secretion at synapses (10, 11). We abolished *munc18-1* expression in mice by homologous recombination (Fig. 1) (12). This resulted in a completely paralyzed organism. Null mutant embryos are alive until birth, but die immediately after birth, probably because they cannot breathe (13).

**Fig. 1.** Generation of mice lacking *munc18-1*. (A) Gene structure of wild-type *munc18-1* (wt) and after homologous recombination (null). Boxes indicate exons with encoding amino acid numbers above. Five exons are replaced with a neomycin resistance gene (NEO<sup>R</sup>). Arrow pairs indicate PCR primers for genotyping. The top arrow indicates the Northern probe, and the grey boxes indicate Southern probes. H, Hind III; E, Eco RI; B, Bam HI; K, Kpn I; and S, Sma I. (B) Southern blot of *munc18-1* mutants. Eco RI-digested genomic DNA from wild types (+/+), heterozygotes (+/-), and homozygotes (-/-) was hybridized with probe 1. Two independent mouse lines (called 18 and 23 after the ES cell clone) contained identical deletions. (C) RNA blot of *munc18-1* mRNA in wild types and homozygotes around birth. (D) Immunoblot analysis of *munc18-1* at E18 in all genotypes. Blots were probed with a *munc18-1*-specific monoclonal antibody (left) or with a general *munc18* polyclonal antibody (right) to detect possible compensatory changes in other *munc18* isoforms. RBH, rat brain homogenate.

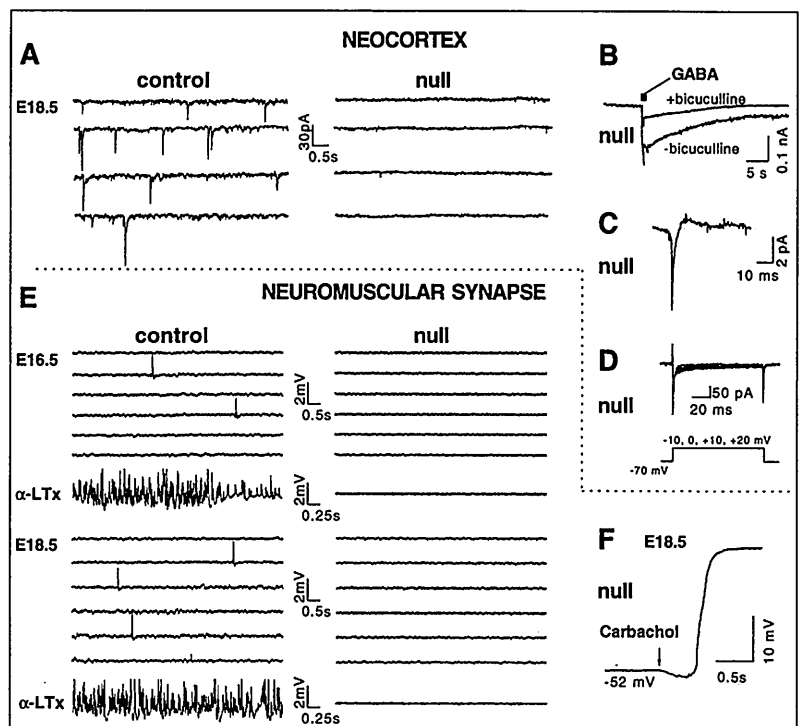


<sup>1</sup>Molecular Neuroscience, Rudolf Magnus Institute, University of Utrecht Medical Centre, Utrecht, Netherlands. <sup>2</sup>Center for Basic Neuroscience, Howard Hughes Medical Institute, and Department of Molecular Genetics, University of Texas Southwestern Medical Center, Dallas, TX 75235, USA. <sup>3</sup>Departments of Neurology and Physiology, Leiden University Medical Centre, Leiden, Netherlands. <sup>4</sup>Department of Neurophysiology, Institute for Neurosciences, Vrije Universiteit Amsterdam, Netherlands. <sup>5</sup>Howard Hughes Medical Institute and Department of Biochemistry, University of Texas Southwestern Medical Center, Dallas, TX 75235, USA. <sup>6</sup>Department of Cell Biology and Immunology, Vrije Universiteit Amsterdam, Netherlands. <sup>7</sup>Department of Cell Biology, University of Utrecht, Utrecht, Netherlands.

\*To whom correspondence should be addressed. E-mail: m.verhage@med.uu.nl (M.V.); tsudho@mednet.swmed.edu (T.C.S.)

†Present address: Center for Physiology and Pathophysiology, University of Göttingen, Germany.

**Fig. 2.** *munc18-1*-deficient mice lack synaptic neurotransmitter release. (A) Whole-cell voltage clamp recordings from neocortical neurons in slices at E18. Wild-type neurons showed frequent spontaneous synaptic events ( $5.4 \pm 2.4 \text{ min}^{-1}$ ; mean  $\pm$  SEM,  $n =$  three animals and four recordings), whereas neurons in null mutant slices were completely devoid of such activity ( $n =$  three animals and five recordings; total recording time, 30.8 min). (B)  $\gamma$ -Aminobutyric acid (GABA) iontophoresis (1 M, 200 to 400 nA, 10 to 20 pulses for 0.1 s at 4 Hz) in mutant brain slices caused a normal postsynaptic response, sensitive to bicuculline (20  $\mu\text{M}$  in bath). (C) Spontaneous action potentials in the cell-attached mode. (D) Voltage-gated inward ion currents in whole-cell mode in mutant cells. (C) and (D) indicate that we recorded from neurons, not glial cells. (E) Intracellular recordings in diaphragm muscle fibers from control and null mutant littermates. Control embryos exhibited miniature endplate potentials (MEPPs):  $5.4 \pm 0.6 \text{ min}^{-1}$  at E15 (one animal, nine fibers  $\pm$  SEM);  $1.3 \pm 0.3 \text{ min}^{-1}$  at E16 (two animals, five fibers per animal  $\pm$  SEM); and  $2.8 \pm 0.6 \text{ min}^{-1}$  at E18 (two animals, five fibers per animal  $\pm$  SEM). No MEPPs were detected in *munc18-1*-deficient mice at E15 (nine fibers; total recording time, 18.8 min), E16 (five fibers, 21.5 min recording), or E18 (11 fibers, 35.5 min recording).  $\alpha$ -Latrotoxin (4 nM) induced massive neurotransmitter release in controls but was completely ineffective in mutant muscle fibers. (F) Carbachol (1 mM) elicited a strong postsynaptic potential and contraction in E18 mutant muscle fibers.



REPORTS

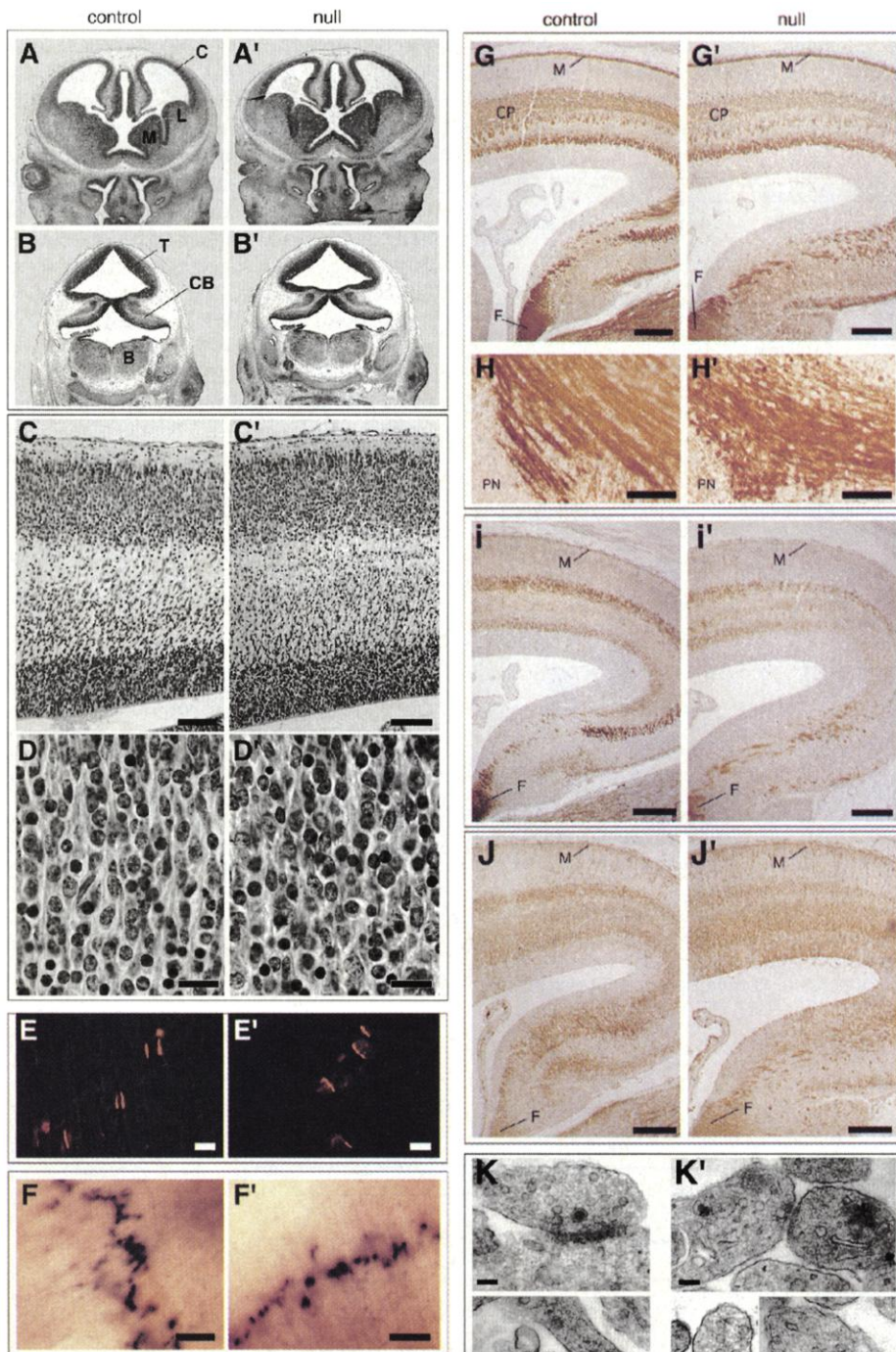


**Fig. 3.** Correct assembly of the brain in the absence of neurotransmitter secretion. (A and B) Coronal sections of developing brains at E12 from control [(A) and (B)] and null mutant [(A') and (B')] littermates stained with hematoxylin and eosin. (A) is located anterior to (B). C, cortex; CB, cerebellar anlage; T, tectum; L and M, lateral and medial ganglionic eminence; B, brainstem. (C and D) Normal architecture of the neocortex in null mutant mice at E18. Scale bars, 100  $\mu$ m in (C), 20  $\mu$ m in (D). (E) Clustering of acetylcholine receptors in the diaphragm neuromuscular junction visualized with fluorescent  $\alpha$ -bungarotoxin at E18. Scale bars, 15  $\mu$ m. (F) Accumulation of acetylcholinesterase at synaptic sites in the diaphragm at E18. Scale bars, 250  $\mu$ m. (G and H) GAP-43 staining of the developing cortex at E18 (H) and the giant fiber pathway above the pontine nucleus (PN). M, marginal zone (synaptic layer); F, fimbria fornix fiber bundle. Scale bars, 200  $\mu$ m in (G), 20  $\mu$ m in (H). (I and J) Synapsin I (I) and synaptobrevin/VAMP II (J) staining at E18, showing that synaptic vesicle markers are transported to the synaptic layer (M). Scale bars, 200  $\mu$ m. (K) Synapses in the neocortex marginal zone at E16 showing apparently normal synaptic structures in the null mutants (K') with clustered and docked synaptic vesicles near or at presynaptic active zones and postsynaptic densities. Scale bars, 50 nm.

Synaptic transmission can normally be detected as soon as a synapse is formed. In the mammalian neocortex, the first synapses are observed at embryonic day 16 (E16) (14). Electron microscopy of the marginal zone in control embryos (13) confirmed the presence of a few synapses at E16 (15), although we did not detect synaptic secretion events in neocortical slices at E17 (16). However, at E18, synaptic events were readily observed (Fig. 2A). In contrast, null mutants lacked synaptic events (Fig. 2A). Nevertheless, in these mutants postsynaptic receptors were functional (Fig. 2B), spontaneous action potentials were occasionally observed (Fig. 2C), and ion channels showed normal properties (Fig. 2D). To study neurotransmitter secretion in a different, earlier developing synapse, we investigated the diaphragm neuromuscular junction between E15 and E18 (16). In these synapses too, synaptic events were detected in controls, but null mutants lacked synaptic events at E15, E16, and E18 (Fig. 2E). Application of  $\alpha$ -latrotoxin or electrical nerve stimulation strongly stimulated synaptic transmission in control littermates but caused no response in null mutants, although their postsynaptic receptors were functional (Fig. 2, E and F).

Despite the general, complete, and permanent loss of synaptic transmission in the knockout mice, their brains were assembled correctly (Fig. 3). Neuronal proliferation, migration, and differentiation into specific brain areas were unaffected. At E12, brains from null mutant and control littermates were morphologically indistinguishable (Fig. 3, A and B) (17). At birth, late-forming brain areas such as the neocortex appeared identical in null mutant and control littermates, including a distinctive segregation of neurons into cortical layers (Fig. 3, C and D). Furthermore, fiber pathways were targeted correctly in null mutants: The growth cone marker GAP-43 showed a normal distribution, including marked staining of fiber bundles and synaptic layers (Fig. 3, G and H). Immunolabeling patterns for presynaptic markers were similar in mutant and control littermates (Fig. 3, I and J). The levels of several synaptic proteins were also normal in the mutants, suggesting that neuronal differentiation and synthesis of synaptic components proceeded normally (18). Moreover, synapses were readily formed in null mutants, being already present in the neocortex at E16 at the onset of synaptogenesis (14). These synapses exhibited all the signs of synaptic complexes (Fig. 3I). The synapses in controls and knockouts contained the same numbers of total and docked synaptic vesicles (19). Other aspects of the ultrastructure were also indistinguishable between mutants and controls (20).

Formation of neuromuscular synapses requires precise navigation of nerve terminals over large distances. At the neuromuscular junction, nerve terminals secrete signals such as

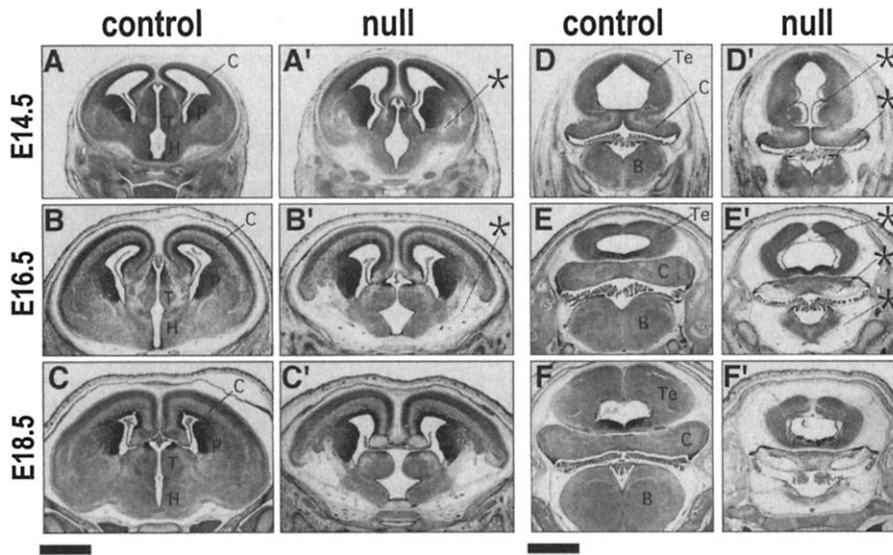


**Fig. 4.** Massive neurodegeneration after assembly of the neuronal networks. Coronal brain sections of control [(A) through (F)] and null mutant [(A') through (F')] littermates between E14 and birth. The asterisks identify locations where degeneration starts. Scale bars, 1 mm. B, brainstem; H, hypothalamus; P, putamen; T, thalamus; Te, tectum. In (A) to (C), C indicates cortex; in (D) to (F), C indicates cerebellar anlage.

agrin that induce clustering of postsynaptic acetylcholine receptors and acetylcholinesterase (21, 22). Thus, assembly of receptor and enzyme clusters provides a sensitive measure of pathfinding and synaptogenesis.  $\alpha$ -Bungarotoxin and acetylcholinesterase staining of diaphragm muscles revealed clear receptor and enzyme clusters in null mutant mice (Fig. 3, E and F) (23), which suggests that long-range axonal pathfinding and initial synapse formation must have occurred.

After initial brain assembly, extensive cell death of mature neurons was observed in the null mutants (Fig. 4), occurring first in lower brain areas that mature and form synapses relatively early (Fig. 4, D through F). For example, at E12 the brainstems of null mutant and control littermates were morphologically similar (Fig. 3B). Although this area expanded further in controls, the neurons disappeared in null mutants until, at E18, the lower brainstem was almost completely lost. Degeneration occurred later in the midbrain and basal forebrain (Fig. 4, A through C). Brain areas that develop last,

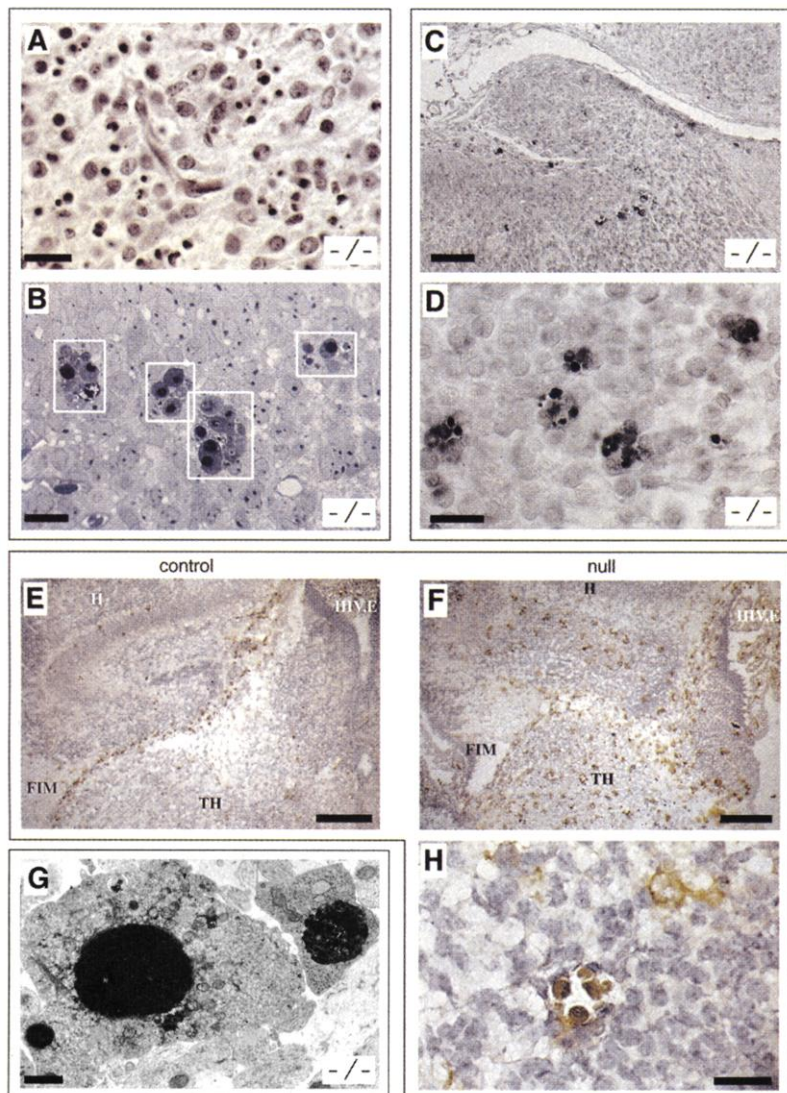


**Fig. 5.** Neurons undergo massive apoptosis after initial synaptogenesis. (A and B) Cell death exhibiting dark indented nuclei in the thalamus of null mutant mice at E18 stained with hematoxylin and eosin (A) or methylene blue (B) is shown. Scale bars, 20  $\mu$ m. (C and D) TUNEL staining of the null mutant hippocampus. Scale bars, 200  $\mu$ m in (C), 20  $\mu$ m in (D). (E, F, and H) Activated macrophage staining in the hippocampus and thalamus at E18 with F4/80 antibody (25). In controls, activated macrophages were largely restricted to the ventricles (E). In the null mutants, dense staining was observed throughout the tissue and colocalized with apoptotic cell bodies (F and H) that were probably engulfed by macrophages (H). H, hippocampus; FIM, fimbria; TH, thalamus. Scale bars, 200  $\mu$ m in (E) and (F), 20  $\mu$ m in (H). (G) Electron micrograph of an affected neuron in the null mutant thalamus, showing compacted chromatin inside the nucleus. Scale bar, 3  $\mu$ m.

especially the neocortex, were indistinguishable from those of controls at birth. The degeneration in the mutant brains exhibited all characteristics of apoptosis: Apoptotic bodies were readily observed with standard histology (Fig. 5, A and B). These were positive in TUNEL staining (Fig. 5, C and D) (24). Apoptotic bodies contained condensed chromatin (Fig. 5G). A final phase of these degenerations was accompanied by abundant staining for activated macrophages (Fig. 5, E, F, and H) (25) and disintegration of lower brain areas around birth (Fig. 4).

Thus, a gene deletion that abolishes presynaptic secretion and therewith synaptic transmission allows an apparently normal initial assembly of the brain. This is quite unlike gene deletions for developmental factors, which generally result in some defect in the assembly of the brain (agenesis) (26). Ablation of *munc18-1* renders the brain synaptically silent, identifying *munc18-1* as the currently most upstream essential protein in neurotransmitter release. Axons in the *munc18-1* mutants extend normally and form precise connections between widely separated brain areas, and synapses develop that look morphologically normal. It has been proposed that early spontaneous activity of neurons results in  $Ca^{2+}$  transients and may be critical for proper differentiation and pathfinding (27). However, this spontaneous activity must act by a mechanism that does not require synaptic neurotransmitter release, because *munc18-1*-deficient neurons differentiate normally, exhibit spontaneous action potentials, and perform apparently normal pathfinding. After synaptic assembly of the brain, activity-dependent selection is thought to maintain certain synaptic connections for adult life, whereas others are discarded (1, 2). Our data indicate that the neuronal networks are synaptically assembled and reach the selection stage without synaptic transmission, but cannot persist without it. When synaptic transmission is absent in newly established synaptic connections, these synapses degenerate and neurons go into apoptosis. Finally, our data indicate that the distribution of membrane to the growing axon tip and the release of signals that allow correct axon targeting depend on different molecular mechanisms than neurotransmitter release by regulated exocytosis of synaptic vesicles.

References and Notes

1. G. M. Shepherd, *The Synaptic Organization of the Brain* (Oxford Univ. Press, New York, ed. 3, 1990).
2. R. Keynes and G. M. W. Cook, *Cell* **83**, 161 (1995); C. S. Goodman, *Annu. Rev. Neurosci.* **19**, 341 (1996); M. Tessier-Lavigne and C. S. Goodman, *Science* **274**, 1123 (1996).
3. S. Catsicas, G. Grenningloh, E. M. Pich, *Trends Neurosci.* **17**, 368 (1994); A. Osen-Sand et al., *J. Comp. Neurol.* **367**, 222 (1996); L. C. Williamson and E. A. Neale, *J. Neurosci. Res.* **52**, 569 (1998).
4. T. L. Fletcher, P. L. Cameron, P. De Camilli, G. Banker, *J. Neurosci.* **11**, 1617 (1991); C. Daly and E. B. Ziff, *J. Neurosci.* **17**, 2365 (1997).

5. M. Matteoli, K. Takei, M. S. Perin, T. C. Südhof, P. De Camilli, *J. Cell Biol.* **117**, 849 (1992); M. Igarashi, M. Tagaya, Y. Komiya, *J. Neurosci.* **17**, 1460 (1997); A. Osen-Sand et al., *Nature* **364**, 445 (1993).
6. Y. A. Sun and M.-M. Poo, *Proc. Natl. Acad. Sci. U.S.A.* **84**, 2540 (1987); Z. P. Xie and M.-M. Poo, *Proc. Natl. Acad. Sci. U.S.A.* **83**, 7069 (1986); S. Coco, C. Verderio, P. De Camilli, M. Matteoli, *J. Neurochem.* **71**, 1987 (1998).
7. T. C. Südhof, *Nature* **375**, 645 (1995); N. Calakos and R. H. Scheller, *Physiol. Rev.* **76**, 1 (1996).
8. R. Fernandez-Chacon and T. C. Südhof, *Annu. Rev. Physiol.* **61**, 753 (1999).
9. M. Geppert et al., *Cell* **79**, 717 (1994); I. Augustin, C. Rosenmund, T. C. Südhof, N. Brose, *Nature* **400**, 457 (1999).
10. Munc18-1 is also called Munc18a, N-sec1, or Rb-sec1 [Y. Hata, C. A. Slaughter, T. C. Südhof, *Nature* **366**, 347 (1993); Y. Hata and T. C. Südhof, *J. Biol. Chem.* **270**, 13022 (1995); J. Pevsner, S. C. Hsu, R. H. Scheller, *Proc. Natl. Acad. Sci. U.S.A.* **91**, 1445 (1994); E. P. Garcia, E. Gatti, M. Butler, J. Burton, P. De Camilli, *Proc. Natl. Acad. Sci. U.S.A.* **91**, 2003 (1994); J. T. Tellam, S. McIntosh, D. E. James, *J. Biol. Chem.* **270**, 5857 (1995)].
11. M. Verhage et al., *Neuron* **18**, 453 (1997); M. Okamoto and T. C. Südhof, *J. Biol. Chem.* **272**, 31459 (1997); S. Butz, M. Okamoto, T. C. Südhof, *Cell* **94**, 773 (1998).
12. Two murine genomic *munc18-1* clones in  $\lambda$ -FIX were used to construct a targeting vector to replace five exons of the *munc18-1* gene by a neomycin resistance gene flanked by an 11.5-kb long arm and a 1.4-kb short arm, which in turn is flanked by two copies of the *Herpes simplex* thymidine kinase gene. Embryonic stem (ES) cells ("G-cells", gift of J. Herz, Dallas, TX) were electroporated [T. W. Rosahl et al., *Cell* **75**, 661 (1993)] and analyzed by polymerase chain reaction (PCR) with oligonucleotide A (outside sense primer CCGTACTTGGGGATTGAACCCAGGC), oligonucleotide B (neomycin antisense primer to detect the mutant allele GGATGCGGTGGCTCTATG-GCTTCTGA), and oligonucleotide C (inside antisense primer to detect the wild-type allele AAAGGAA-CGGGGTGGAGGGAGAGA). Homologously recombined clones were confirmed by Southern blotting with outside probes (A and B in Fig. 1A). Two positive ES cell clones were injected into blastocysts, generating highly chimeric mice that transmitted the mutation through the germ line. The genotypes of litters from heterozygote matings exhibited a Mendelian distribution.
13. Throughout this study, mouse embryos were obtained by caesarean section of pregnant females from timed heterozygous matings. Littermates were analyzed without prior genotyping. Null mutant animals had a beating heart until birth. Data from wild-type and heterozygous embryos were pooled as the control group after pilot experiments revealed no differences between these groups. Animals were housed and bred according to institutional, Dutch, and U.S. governmental guidelines.
14. N. König, G. Roch, R. Marty, *Anat. Embryol.* **148**, 73 (1975).
15. Brains of embryos at E16 to E18 were immersed in 1% paraformaldehyde, 2% glutaraldehyde, and 0.05 M sodium cacodylate buffer (pH 7.4) for 2 days at 4°C; postfixed in 1%  $OsO_4$  in 0.1 M cacodylate buffer; dehydrated; and embedded in epoxy resin. Ultrathin (90 nm) sections were contrasted with uranyl acetate and lead citrate. Synapses were defined as structures containing one or more 30- to 50-nm vesicles in the vicinity of a pre- and postsynaptic specialization.
16. Cortical slices (400  $\mu$ m) at E17 and E18 were prepared on a Campden vibratome, and whole cell recordings were performed in situ at 33°C and a holding potential of -70 mV [A. B. Brussaard et al., *Neuron* **19**, 1103 (1997)]. Neuromuscular junction recordings were performed on diaphragm nerve and muscle preparations at E15, E16, and E18 using 30- to 40-megohm glass capillary microelectrodes at 26° to 28°C [J. J. Plomp, G. T. H. Van Kempen, P. C. Molenaar, *J. Physiol.* **478**, 125 (1994)]. The phrenic nerve was stimulated with a suction electrode; responses

were recorded intracellularly in muscle fibers at endplates. Thereafter, 1  $\mu$ M tetrodotoxin was added to suppress spontaneous contractions of fibers, which occurred in all genotypes and interfere with the recording of spontaneous events. In control experiments, a micropipette with 1 mM carbachol and a broken tip to allow leakage was brought into the vicinity of the measuring electrode.

17. Mouse embryos (at E12 to E18) were immersed in 71.4% saturated picric acid, 23.8% formalin, and 4.8% acetic acid for 3 days; dehydrated; and embedded in paraffin. Brain sections (5  $\mu$ m) were stained with hematoxylin and eosin. For immunohistochemistry, sections were rehydrated, microwaved in 0.1% Froggy detergent in 50 mM tris-buffered saline (TBS) (pH 7.5) four times for 5 min, and washed three times in TBS. Endogenous peroxidase was blocked with 0.6%  $H_2O_2$  in 100% methanol for 30 min at room temperature. Sections were washed again three times in TBS and incubated for 1 hour at room temperature in 3% normal goat serum (NGS), 250 mM TBS, 1% BSA, and 0.1% Triton-X-100. For monoclonal antibodies, NGS was replaced by 1% goat anti-mouse serum. Sections were incubated at room temperature with primary antibodies overnight, with biotinylated secondary antibody for 1 hour, with peroxidase-labeled streptavidin-biotin complex for 1 hour, and with 3,3'-diaminobenzidine. For the monoclonal synaptobrevin antibody, the Sternberger PAP-method was used for detection. Antibodies used were 9527 (GAP-43), CL69.1 (synaptobrevin II), and E028 (synapsins). Control experiments omitting primary antibodies confirmed staining specificity. For Fig. 5B, brains were processed as in (15), sectioned at 5  $\mu$ m, and post-stained with methylene blue.
18. Protein quantification in total brain homogenates from E18 embryos was performed by quantitative immunoblotting using  $^{125}I$ -labeled secondary antibodies [H. McMahon et al., *Proc. Natl. Acad. Sci. U.S.A.* **93**, 4760 (1996)]. To correct for degeneration in the null mutants (Figs. 4 and 5), protein levels were corrected with hexokinase, guanosine diphosphate disassociation inhibitor, and calmodulin as internal standards. Relative protein levels in knockout animals as compared to wild-type animals (100%) were as follows (mean  $\pm$  SEM from triplicate determinations): synaptophysin, 96  $\pm$  14%; synaptobrevin II, 98  $\pm$  12%; rab3A/C, 87  $\pm$  16%; GAP-43, 95  $\pm$  10%; and NMDA receptor, 101  $\pm$  5% (K. J. De Vries et al., in preparation).
19. Quantification of electron micrographs from the neocortex marginal zone at E16 was as follows. Synaptic vesicles per synapse: wild type, 5.2  $\pm$  2.5; null mutant, 3.9  $\pm$  1.7. Docked synaptic vesicles per synapse: wild type, 2.1  $\pm$  1.4; null mutant, 1.9  $\pm$  1.1 (three animals, three sections per animal  $\pm$  SEM; one section =  $\pm$  1700  $\mu$ m<sup>2</sup>).
20. Axon, dendrite, and soma morphology were from A. S. Maia, H. J. Geuze, and M. Verhage, unpublished observations.
21. J. R. Sanes and J. W. Lichtman, *Annu. Rev. Neurosci.* **22**, 389 (1999).
22. S. DelaPorte et al., *Eur. J. Neurosci.* **10**, 1631 (1998)
23. Acetylcholine receptors and acetylcholinesterase were analyzed in whole-mount diaphragm neuromuscular junctions at E18. Diaphragms were fixed (for 90 min in 2% paraformaldehyde in PBS) and rinsed (for 30 min in 0.1 M glycine in PBS). After 15 min of preincubation in 0.5% Triton X-100 and 1% bovine serum albumin (BSA) in PBS, tetramethyl rhodamine isothiocyanate-labeled  $\alpha$ -bungarotoxin (1  $\mu$ g/ml) was added, and diaphragms were incubated overnight at 4°C. Diaphragms were washed, mounted in Dabco-Mowiol, and analyzed with confocal laser microscopy. Acetylcholinesterase was stained in unfixed diaphragms for 1 hour with 0.5 mM 5-bromo indoxylacetate [S. J. Holt and R. F. J. Withers, *Nature* **170**, 1012 (1952)].
24. For terminal deoxytransferase-mediated deoxy-uridine triphosphate nick end labeling (TUNEL) staining, paraffin sections (17) were rehydrated; incubated with 1%  $H_2O_2$  in methanol for 5 min; microwaved in 1%  $ZnSO_4$  and 1% Triton in 10 mM PBS at 45°C and 150 W for 5 min; rinsed at 4°C; and microwaved and rinsed again. Sections were stained with the In Situ Cell Death Detection Kit, peroxidase-conjugated converter enzyme peroxi-

dase, and 3,3-diaminobenzidine-Ni<sup>3+</sup>. As controls, either TUNEL enzyme or peroxidase converter enzyme was omitted.

25. Cryosections of embryonal mouse heads (10  $\mu$ m) were fixed for 10 min in acetone, incubated with monoclonal antibody F4/80 [undiluted cell supernatant, D. A. Hume and S. Gordon, *J. Exp. Med.* **157**, 1704 (1983)] for 1 hour at room temperature, rinsed three times with PBS, incubated with peroxidase-coupled rabbit antibody to mouse secondary antibody for 1 hour, rinsed again three times with PBS,

and stained with 3,3-diaminobenzidine. Sections were washed in 0.9% NaCl, incubated in CuSO<sub>4</sub> for 30 min, washed again, immersed in hematoxylin, and dehydrated.

26. M. Hallonet *et al.*, *Development* **125**, 2599 (1998); Y. Tanabe and T. M. Jessell, *Science* **274**, 1115 (1996); A. L. Joyner, *Trends Genet.* **12**, 15 (1996).

27. T. M. Gomez and N. C. Spitzer, *Nature* **397**, 350 (1999); L. D. Milner and L. T. Landmesser, *J. Neurosci.* **19**, 3007 (1999).

28. The authors are grateful to G. Posthuma, D. T. Nolan,

R. Fernandez-Chacon, L. C. van Halewijn, L. Lundquist, T. Broers-Vendrig, E. Borowicz, I. Leznicki, and A. Roth for assistance; R. Jahn, J. Herz, B. Oestreicher, and Y. Hata for supply of materials; and J. P. H. Burbach, F. H. Lopes da Silva, M. S. Brown, and J. L. Goldstein for discussions. We are particularly grateful to W. H. Gispen for his help and support. Supported by the Netherlands Organization for Scientific Research (NWO), the Keck Foundation, the Perot Family Foundation, and the David de Wied Foundation.

3 November 1999; accepted 14 December 1999

## A Subclass of Ras Proteins That Regulate the Degradation of I $\kappa$ B

Craig Fenwick,<sup>1\*</sup> Soon-Young Na,<sup>2,4\*</sup> Reinhard E. Voll,<sup>1</sup>  
Haihong Zhong,<sup>1</sup> Sunh-Young Im,<sup>3,5</sup> Jae Woon Lee,<sup>4,5†</sup>  
Sankar Ghosh<sup>1†</sup>

Small guanosine triphosphatases, typified by the mammalian Ras proteins, play major roles in the regulation of numerous cellular pathways. A subclass of evolutionarily conserved Ras-like proteins was identified, members of which differ from other Ras proteins in containing amino acids at positions 12 and 61 that are similar to those present in the oncogenic forms of Ras. These proteins,  $\kappa$ B-Ras1 and  $\kappa$ B-Ras2, interact with the PEST domains of I $\kappa$ B $\alpha$  and I $\kappa$ B $\beta$  [inhibitors of the transcription factor nuclear factor kappa B (NF- $\kappa$ B)] and decrease their rate of degradation. In cells,  $\kappa$ B-Ras proteins are associated only with NF- $\kappa$ B:I $\kappa$ B $\beta$  complexes and therefore may provide an explanation for the slower rate of degradation of I $\kappa$ B $\beta$  compared with I $\kappa$ B $\alpha$ .

The transcription factor NF- $\kappa$ B plays an important role in the expression of a large number of inducible genes. In unstimulated cells, NF- $\kappa$ B remains in an inactive form in the cytoplasm bound to a member of the I $\kappa$ B family of inhibitors. Exposure of cells to various stimuli—including cytokines [such as tumor necrosis factor (TNF) and interleukin-1 (IL-1)], lipopolysaccharides, and ultraviolet light—results in the activation of signal transduction pathways that lead to the phosphorylation and degradation of the I $\kappa$ B proteins. The released NF- $\kappa$ B then translocates to the nucleus where it up-regulates the synthesis of genes involved in immune and inflammatory responses, including cytokines and adhesion molecules (1).

Another class of proteins that play a very important role in the transduction of cell surface signals is small guanosine triphosphatases (GTPases) such as Ras, Rap, Ral, and Rho (2, 3). The Ras family (H-ras, K-ras, and N-ras) became the focus of intense interest when it was discovered that specific mutations in these proteins were associated with ~30% of all human tumors, including 50% of colon and 90%

of pancreatic adenocarcinomas (4, 5). These mutations, which lock the Ras proteins in a constitutively active, guanosine triphosphate (GTP)-bound form, are almost exclusively confined to three critical positions, 12, 13, and 61 (6). The ability of Ras proteins to transduce growth-stimulatory signals is dependent on their localization to the inner side of the plasma membrane and requires farnesylation of their COOH-termini (7).

Oncogenic Ras and the Rho GTPases can activate NF- $\kappa$ B, although the details of the signal transduction pathways responsible remain to be identified (8, 9). Ras-activated NF- $\kappa$ B is proposed to act as an antiapoptotic factor that helps prevent transformed cells from undergoing p53-independent apoptosis (8). In an attempt to further explore the regulation of NF- $\kappa$ B signaling, we used yeast two-hybrid interaction screens with I $\kappa$ B proteins as bait to identify interacting molecules. In one such screen, using the COOH-terminal portion of I $\kappa$ B $\beta$ , I $\kappa$ B $\beta$  $\Delta$ 1 (amino acids 173 to 361), as bait, we isolated a series of mouse cDNAs (10), including a Ras-like protein that we named  $\kappa$ B-Ras1 (for I $\kappa$ B-interacting Ras-like protein 1). In yeast,  $\kappa$ B-Ras1 specifically interacted with full-length I $\kappa$ B $\beta$  and I $\kappa$ B $\beta$  $\Delta$ 1, but not with the I $\kappa$ B-like protein Bcl-3, the NF- $\kappa$ B subunits p50 and p65, or the transcription factors Myc and Bicoid (11–13). A full-length human cDNA clone of  $\kappa$ B-Ras1 was then isolated, in which the initiator methionine is preceded by an in-frame stop codon. Using the sequence of  $\kappa$ B-Ras1, we

searched the expressed sequence tag (EST) databases and identified a related protein that was named  $\kappa$ B-Ras2. Polymerase chain reaction was used to isolate the full-length human  $\kappa$ B-Ras2 clone, which encodes a protein highly related to  $\kappa$ B-Ras1 (71% identity, 85% similarity) (Fig. 1A). In vitro translation of the  $\kappa$ B-Ras2 cDNA produced a protein of about 22 kD, which is slightly smaller than the human  $\kappa$ B-Ras1 protein (Fig. 1B). In addition, a search of *Drosophila* EST databases identified a highly conserved homolog to  $\kappa$ B-Ras (40% identity and 68% similarity to human  $\kappa$ B-Ras1; Fig. 1A). This is of particular interest, considering that homologs to both components of NF- $\kappa$ B and Ras are present in *Drosophila*.

Comparison of the sequences of the mammalian  $\kappa$ B-Ras1 and  $\kappa$ B-Ras2 with other small GTPases reveals their overall similarity, for example, 30% identity and 49% similarity to human K-ras (Fig. 1C) (14, 15). Their assignment as a distinct subgroup of Ras-like proteins becomes apparent when small GTPases are sorted and classified with a dendrogram (Fig. 1D) (16). The major difference between  $\kappa$ B-Ras and other Ras proteins (H-, K-, and N-Ras) is the lack of COOH-terminal membrane attachment sequences (Cys-a-a-X sequences, where “a” is any aliphatic amino acid and “X” is any amino acid) and the presence of alanine or leucine at position 13 (instead of glycine) and leucine at position 65 (instead of glutamine) (equivalent to positions 12 and 61, respectively, in H-Ras) (Fig. 1C) (14, 15). The presence of alanine or leucine at position 12 and leucine at position 61 locks the known Ras proteins into a deregulated, active, GTP-bound conformation and underlies their oncogenicity (17, 18). We therefore tested whether  $\kappa$ B-Ras proteins also bound GTP. We produced COOH-terminal His-tagged  $\kappa$ B-Ras1 protein in a bacterial overexpression system and used the GTP-binding protein Sec4 as a positive control for a nucleotide-binding assay (19). The  $\kappa$ B-Ras1 protein specifically bound GTP, but not adenosine triphosphate (ATP) (Fig. 1E). The expression of  $\kappa$ B-Ras1 and  $\kappa$ B-Ras2 in various human tissues was examined with multiple tissue Northern (RNA) blot analysis. Both human  $\kappa$ B-Ras1 and  $\kappa$ B-Ras2 are widely expressed and are encoded by mRNAs of 1.6 and 2.5 kb, respectively (Fig. 1F). The nonoverlapping expression of the two  $\kappa$ B-Ras proteins suggests that they might have distinct functions in different tissues.

<sup>1</sup>Section of Immunobiology and Department of Molecular Biophysics and Biochemistry, Howard Hughes Medical Institute, Yale University School of Medicine, New Haven, CT 06510, USA. <sup>2</sup>Department of Biology, <sup>3</sup>Department of Microbiology, <sup>4</sup>Center for Ligand and Transcription and <sup>5</sup>Hormone Research Center, Chonnam National University, Kwangju 500-757, Korea.

\*These authors contributed equally to this work.  
†To whom correspondence should be addressed.